Chemical Engineering Science 66 (2011) 3020–3029

Contents lists available at ScienceDirect

Chemical Engineering Science

journal homepage: www.elsevier.com/locate/ces

Integral methods for flow in a conical centrifuge

Digby D. Symons *

University of Cambridge, Department of Engineering, Trumpington Street, Cambridge CB2 1PZ, United Kingdom

ARTICLE INFO

Article history:
Received 6 August 2010
Received in revised form
25 March 2011
Accepted 5 April 2011
Available online 13 April 2011

Keywords::
Centrifugation
Films
Fluid mechanics
Laminar flow
Mathematical modelling
Spinning cone

ABSTRACT

A set of through-thickness averaged equations for momentum and strain rate are derived for the problem of axi-symmetric free-surface flow within a spinning cone. The expressions are independent of the choice of constitutive law and can therefore be used for modeling the flow of a variety of materials within an industrial conical centrifuge. By assuming a through-thickness velocity profile the distribution of flow thickness and average velocity over the internal surface of the cone can be obtained. The approach has been validated for thin Newtonian viscous flow by comparison with full three-dimensional solutions of the Navier–Stokes equations obtained with a commercial CFD package. The averaged equations provide an accurate prediction of the flow thickness, velocity and the length of the zones of influence of inlet and outlet boundary conditions.

© 2011 Elsevier Ltd. All rights reserved.

1. Introduction

This paper concerns the governing equations for steady, axi-symmetric, free-surface flow within a conical centrifuge. Such a flow may be found in a variety of industrial applications such as spinning cone distillation columns, centrifugal evaporators and conical centrifugal filters. The objective is to present a set of equations for strain rate and momentum written in terms of through-thickness averaged quantities. These equations are independent of the choice of constitutive law and therefore provide a computationally efficient method for modeling the flow of a variety of materials in a conical centrifuge.

A spherical co-ordinate system (r,θ,ϕ) in an Eulerian reference frame is adopted to describe the flow in the cone (see Fig. 1). The cone has apex angle 2β and spins about a vertical axis with a constant angular velocity Ω.

1.1. Prior work

The problem of a free-surface flow in a rapidly spinning cone has been analyzed by Bruin (1969) and Makarytchev et al. (1997), the latter correcting mistakes in the earlier publication. Both papers consider a Newtonian viscous, laminar flow where the film thickness h is much smaller than the radial distance r. Boundary-layer approximations are given for the Navier–Stokes and continuity equations in which the through-thickness velocity component u_θ is assumed to be much smaller than either the radial u_r or circumferential u_ϕ components. Algebraic solutions for the radial variation of film thickness $h(r)$ and the through-thickness velocity profile (the θ-dependence of u_r, u_θ and u_ϕ) are presented for the case of very high speed rotation of the cone where the centrifugal acceleration dominates.

Further work by Makarytchev et al. (1998) identified the radial structure (r-dependence) and regimes of liquid film flow in a spinning cone. A key dimensionless parameter is the Rossby number

$$Ro = \frac{\overline{u}_r}{\Omega r \sin\beta}, \tag{1}$$

where $\overline{u}_r$ is the mean radial velocity of the film flow. Three radial zones may be identified for a thin liquid film: an inertial zone, where $Ro \sim 1$; a Coriolis zone, where $Ro < 1$; and a centrifugal zone, where $Ro \ll 1$. The boundaries between these zones are indicated by the limits of applicability of successive approximations of the Navier–Stokes equations: in the Coriolis zone an inertial term of the order of Ro^2 may be neglected, whereas in the centrifugal zone a Coriolis term of the order of Ro may also be omitted. Whether only one, two or all three of these flow zones exist in a particular flow depends on the flow parameters and centrifuge dimensions.

In an inertial zone the film thickness h exceeds the Ekman layer thickness

$$h_E = \sqrt{\frac{\nu}{\Omega \sin\beta}}, \tag{2}$$

where $\nu = \mu/\rho$ is the kinematic viscosity of the liquid. The flow in the inertial zone therefore has a through-thickness structure with a

* Tel.: +44 1223 760502; fax: +44 1223 332662.
E-mail address: digby.symons@eng.cam.ac.uk

0009-2509/$ - see front matter © 2011 Elsevier Ltd. All rights reserved.
doi:10.1016/j.ces.2011.04.006

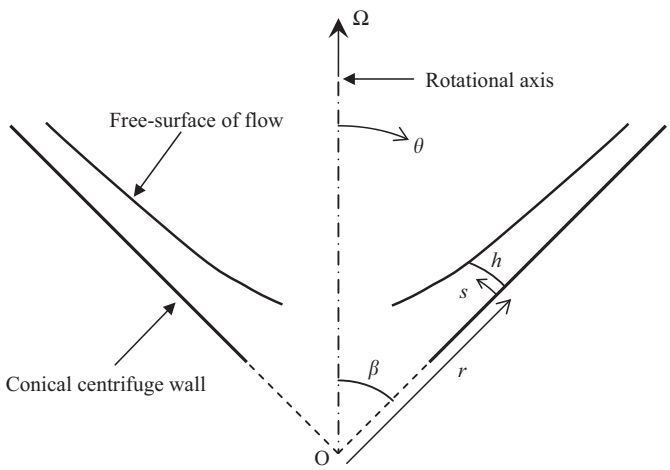

Fig. 1. Cross section of conical centrifuge.

viscous boundary layer of approximate thickness h_E in contact with the spinning cone and a "quasi-geostrophic" layer above this in which the motion of the liquid is almost inviscid. However, within the Coriolis and centrifugal zones the film thickness is less than h_E and therefore the whole flow thickness behaves as a viscous boundary layer. In a centrifugal zone this gives a parabolic profile of radial velocity u_r through the flow thickness equivalent to that obtained for laminar Nusselt flow down an inclined plane under the action of gravity. Makarytchev et al. (1997) give analytical expressions for the velocity and film thickness $h(r)$ in both Coriolis and centrifugal zones. However, these results assume the flow to be unaffected by the boundary conditions at either inlet or outlet to the cone (e.g. the geometry of the flow feed or cone exit).

In contrast, the analysis of flow within a conical centrifuge by Bizard et al. (2011) focuses on determining the lengths of the zones of influence of inlet and outlet boundary conditions. This work does not address the details of the velocity and stress distribution within the thickness of the flow, but is instead concerned with determining the radial variation of the mean flow velocity $\overline{u}_r$ (and thus, by continuity, the thickness h of the flow). The analysis assumes that the whole flow is in a centrifugal zone and therefore that the fluid has an angular velocity identical to that of the cone. It is shown that for a wide range of parameters there will be a mid-zone in this flow where the mean flow velocity is insensitive to the inlet or outlet boundary conditions, but dictated by the shear traction at the interface of the fluid and cone. Two possibilities are considered for this basal shear traction: velocity and pressure dependence (intended to model a non-Newtonian paste flow), and a viscous traction proportional to the velocity gradient at the base of a parabolic flow profile. The second case therefore gives an identical result to Makarytchev et al. (1997) for the Nusselt flow film thickness.

The governing equations for mean flow velocity of Bizard et al. (2011) are obtained by consideration of a control volume which covers the whole local thickness of the flow in the cone. The control volume approach may be compared to the integral methods of Bohr et al. (1993) and Watanabe et al. (2003). Bohr and his co-authors also derive equations for the mean velocity of a free-surface flow, but they adopt an integral method of averaging the elemental momentum and continuity equations over the flow depth. The integral equations require an assumption of a velocity profile through the flow thickness. Although the integral method is approximate it is shown to produce satisfactory results, even with large distortions of the free surface. However, the work of Bohr et al. (1993, 2003) concerns circular flows, or flows down an inclined plane, and was not applied to the problem of flow in a conical centrifuge.

In this paper a similar integral approach to that of Bohr is presented for the derivation of through-thickness averaged equations for axi-symmetric free-surface flow in a spinning cone. The equations are independent of constitutive law and allow the influence of inlet and outlet boundary conditions to be modeled. The work advances that of Bizard et al. (2011) by relaxing the *a piori* assumptions of a thin flow and constant angular velocity (i.e. flow in a centrifugal zone), by determining the effect of the assumed flow profile on the averaged flow strain rates and by comparing numerical results for a Newtonian flow to results obtained using commercial CFD (computational fluid dynamics) software.

1.2. Outline of paper

Starting from elemental equations in spherical co-ordinates, through-thickness averaged (integral) equations are derived for free-surface flow in a conical centrifuge. These equations allow for thick flows and are independent of the constitutive law. The particular problem of a thin centrifugal Newtonian flow is then considered. The appropriate choice of inlet and outlet boundary conditions is discussed and the effect of these is demonstrated with numerical results. The results obtained from the integral equations are compared with results obtained using commercial CFD software. The paper concludes with a comparison of CFD results and the theory of Makarytchev et al. (1997) for the through-thickness variation of velocity in a thin film.

2. Derivation of averaged equations for conical flow

2.1. Description of problem

Fig. 1 shows a cross-section through the flow and cone. The flow is axi-symmetric about the vertical axis and is in steady state, thus $\partial/\partial\phi=\partial/\partial t=0$. The flow thickness is measured by the arc-length $h(r)$ from the cone wall at $\theta=\beta$ (i.e. $s=0$) to the free surface at $\theta=\beta-h/r$ (i.e. $s=h$), where $s=r(\beta-\theta)$. The wall is assumed impermeable and the fluid is assumed incompressible with density ρ.

2.2. Elemental relations in spherical Co-ordinates

2.2.1. Strain rates

For the axi-symmetric case the direct strain rates (see e.g. White, 1991) reduce to

$$D_r=\frac{\partial u_r}{\partial r},\quad D_\phi=\frac{u_r}{r}+\frac{u_\theta}{r\tan\theta},\quad D_\theta=\frac{1}{r}\frac{\partial u_\theta}{\partial\theta}+\frac{u_r}{r}, \tag{3}$$

with incompressibility dictating that

$$D_r+D_\phi+D_\theta=0. \tag{4}$$

The shear strain rates are

$$D_{r\theta}=\frac{1}{2}\left[r\frac{\partial}{\partial r}\left(\frac{u_\theta}{r}\right)+\frac{1}{r}\frac{\partial u_r}{\partial\theta}\right],\quad D_{\theta\phi}=\frac{1}{2}\left[\frac{\sin\theta}{r}\frac{\partial}{\partial\theta}\left(\frac{u_\phi}{\sin\theta}\right)\right],\quad D_{r\phi}=\frac{1}{2}r\frac{\partial}{\partial r}\left(\frac{u_\phi}{r}\right). \tag{5}$$

2.2.2. Momentum equations

To retain independence of the constitutive law we write the momentum equations in terms of direct stresses ($\sigma_r,\sigma_\theta,\sigma_\phi$) and shear stresses ($\tau_{r\theta},\tau_{\theta\phi},\tau_{\phi r}$) (see e.g. Fung and Tong, 2001; White, 1991)

$$\frac{1}{r^3}\frac{\partial}{\partial r}(r^3\tau_{r\theta})+\frac{1}{r\sin\theta}\frac{\partial}{\partial\theta}(\sigma_\theta\sin\theta)-\frac{\sigma_\phi}{r\tan\theta}$$

$$= \rho\left[u_r\frac{\partial u_\theta}{\partial r}+\frac{u_\theta}{r}\frac{\partial u_\theta}{\partial\theta}+\frac{1}{r}\left(u_r u_\theta-\frac{u_\phi^2}{\tan\theta}\right)-g\sin\theta\right], \tag{6}$$

$$\frac{1}{r^2}\frac{\partial}{\partial r}(r^2\sigma_r)+\frac{1}{r\sin\theta}\frac{\partial}{\partial\theta}(\tau_{\theta r}\sin\theta)-\frac{1}{r}(\sigma_\phi+\sigma_\theta)$$
$$= \rho\left[u_r\frac{\partial u_r}{\partial r}+\frac{u_\theta}{r}\frac{\partial u_r}{\partial\theta}-\frac{1}{r}(u_\theta^2+u_\phi^2)+g\cos\theta\right], \tag{7}$$

$$\frac{1}{r^3}\frac{\partial}{\partial r}(r^3\tau_{r\phi})+\frac{1}{r\sin^2\theta}\frac{\partial}{\partial\theta}(\tau_{\theta\phi}\sin^2\theta)=\rho\left[u_r\frac{\partial u_\phi}{\partial r}+\frac{u_\theta}{r}\frac{\partial u_\phi}{\partial\theta}+\frac{1}{r}\left(u_r u_\phi+\frac{u_\theta u_\phi}{\tan\theta}\right)\right], \tag{8}$$

where g is the acceleration due to gravity and it is assumed that the cone rotates about a vertical axis.

2.3. Averaging method

To avoid restricting the analysis to thin flows we define the through-thickness average $\bar{f}$ of any function f as an area average

$$\bar{f}\equiv\frac{1}{A}\int f\,dA\equiv\frac{1}{\lambda}\int_{\beta-h/r}^{\beta} f\sin\theta\,d\theta, \tag{9}$$

where $dA=2\pi r^2\sin\theta\,d\theta$, the spherical cross-sectional area of the flow $A=2\pi r^2\lambda$ and $\lambda=2\sin(h/2r)\sin(\beta-h/2r)$. The thickness of the fluid layer is defined by the arc-length h. Note that in the case of a very thin flow where $h/r\ll\beta$ then $\lambda\approx(h/r)\sin\beta$ and this average simplifies to

$$\bar{f}\approx\frac{r}{h}\int_{\beta-h/r}^{\beta} f d\theta=\frac{1}{h}\int_0^h f ds, \tag{10}$$

where $\partial s=-r\partial\theta$.

The justification for the choice of an area average becomes clear if we consider the volumetric flow rate

$$Q=\int u_r dA=2\pi r^2\int_{\beta-h/r}^{\beta} u_r\sin\theta\,d\theta=2\pi r^2\lambda\bar{u}_r. \tag{11}$$

Note that if h/r is small

$$Q\approx 2\pi r h\bar{u}_r\sin\beta. \tag{11a}$$

2.4. Averaged equations

We now apply the averaging method to the strain rates and momentum equations, recalling Leibniz's rule for differentiation under the integral sign, thus

$$\int_{\beta-h/r}^{\beta}\frac{d}{dr}g(r,\theta)\,d\theta=\frac{d}{dr}\int_{\beta-h/r}^{\beta}g(r,\theta)\,d\theta+\frac{1}{r}\left(\frac{h}{r}-\frac{dh}{dr}\right)g(r,\beta-h/r). \tag{12}$$

We will make use of the streamline directions at the free surface and base of the flow. At the free surface ($s=h$)

$$u_\theta|_h\equiv u_\theta(r,\beta-h/r)=\left(\frac{h}{r}-\frac{\partial h}{\partial r}\right)u_r|_h, \tag{13a}$$

where $u_r|_h\equiv u_r(r,\beta-h/r)$. At the base of the flow ($s=0$) the wall is impermeable and thus

$$u_\theta|_0\equiv u_\theta(r,\theta=\beta)=0. \tag{13b}$$

2.4.1. Strain rates

The direct strain rates averaged over the flow thickness are therefore

$$\bar{D}_r=\frac{1}{\lambda}\frac{\partial}{\partial r}(\lambda\bar{u}_r)-\frac{\sin(\beta-h/r)}{\lambda r}\left(\frac{\partial h}{\partial r}-\frac{h}{r}\right)u_r|_h, \tag{14a}$$

$$\bar{D}_\phi=\frac{1}{r}\bar{u}_r+\frac{1}{r}\overline{\frac{u_\theta}{\tan\theta}}, \tag{14b}$$

$$\bar{D}_\theta=\frac{\sin(\beta-h/r)}{\lambda r}\left(\frac{\partial h}{\partial r}-\frac{h}{r}\right)u_r|_h+\frac{1}{r}\bar{u}_r-\frac{1}{r}\overline{\frac{u_\theta}{\tan\theta}}. \tag{14c}$$

Continuity may now be expressed as

$$\bar{D}_r+\bar{D}_\phi+\bar{D}_\theta=\frac{1}{\lambda r^2}\frac{\partial}{\partial r}(\lambda r^2\bar{u}_r)=0. \tag{15}$$

The averaged shear strain rates are

$$\bar{D}_{r\theta}=\frac{1}{2}\left[\frac{r}{\lambda}\frac{\partial}{\partial r}\left(\frac{\lambda}{r}\bar{u}_\theta\right)+\frac{\sin(\beta-h/r)}{\lambda r}\left(\left(\frac{\partial h}{\partial r}-\frac{h}{r}\right)^2-1\right)u_r|_h+\frac{\sin\beta}{\lambda r}u_r|_0-\frac{1}{r}\overline{\frac{u_r}{\tan\theta}}\right], \tag{16a}$$

$$\bar{D}_{\theta\phi}=\frac{1}{2}\left[\frac{1}{r\lambda}(u_\phi|_0\sin\beta-u_\phi|_h\sin(\beta-h/r))-\frac{2}{r}\overline{\frac{u_\varphi}{\tan\theta}}\right], \tag{16b}$$

$$\bar{D}_{\phi r}=\frac{1}{2}\left[\frac{r}{\lambda}\frac{\partial}{\partial r}\left(\frac{\lambda}{r}\bar{u}_\phi\right)-\frac{\sin(\beta-h/r)}{r\lambda}\left(\frac{\partial h}{\partial r}-\frac{h}{r}\right)u_\phi|_0\right]. \tag{16c}$$

2.4.2. Momentum equations

The through-thickness averaged momentum equations are

$$\frac{1}{r^3\lambda}\frac{\partial}{\partial r}(r^3\lambda\overline{\tau_{r\theta}})-\frac{\sin(\beta-\frac{h}{r})}{\lambda r}\left(\frac{\partial h}{\partial r}-\frac{h}{r}\right)\tau_{r\theta}|_h+\frac{\sin\beta}{\lambda r}\sigma_\theta|_0-\frac{\sin(\beta-\frac{h}{r})}{\lambda r}\sigma_\theta|_h-\frac{1}{r}\overline{\frac{\sigma_\phi}{\tan\theta}}$$
$$=\rho\left[\overline{u_r\frac{\partial u_\theta}{\partial r}}+\frac{1}{r}\overline{u_\theta\frac{\partial u_\theta}{\partial\theta}}+\frac{1}{r}\overline{\left(u_r u_\theta-\frac{u_\phi^2}{\tan\theta}\right)}-g\overline{\sin\theta}\right], \tag{17}$$

$$\frac{1}{r^2\lambda}\frac{\partial}{\partial r}(r^2\lambda\overline{\sigma_r})-\frac{\sin(\beta-\frac{h}{r})}{\lambda r}\left(\frac{\partial h}{\partial r}-\frac{h}{r}\right)\sigma_r|_h+\frac{\sin\beta}{\lambda r}\tau_{\theta r}|_0-\frac{\sin(\beta-\frac{h}{r})}{\lambda r}\tau_{\theta r}|_h-\frac{1}{r}\overline{(\sigma_\phi+\sigma_\theta)}$$
$$=\rho\left[\overline{u_r\frac{\partial u_r}{\partial r}}+\frac{1}{r}\overline{u_\theta\frac{\partial u_r}{\partial\theta}}-\frac{1}{r}\overline{(u_\theta{}^2+u_\phi^2)}+g\overline{\cos\theta}\right], \tag{18}$$

$$\frac{1}{r^3\lambda}\frac{\partial}{\partial r}(r^3\lambda\overline{\tau_{\phi r}})-\frac{\sin(\beta-\frac{h}{r})}{\lambda r}\left(\frac{\partial h}{\partial r}-\frac{h}{r}\right)\tau_{\phi r}|_h+\frac{\sin\beta}{\lambda r}\tau_{\theta\phi}|_0-\frac{\sin(\beta-\frac{h}{r})}{\lambda r}\tau_{\theta\phi}|_h+\frac{1}{r}\overline{\frac{\tau_{\theta\phi}}{\tan\theta}}$$
$$=\rho\left[\overline{u_r\frac{\partial u_\phi}{\partial r}}+\frac{1}{r}\overline{u_\theta\frac{\partial u_\phi}{\partial\theta}}+\frac{1}{r}\overline{\left(u_r u_\phi+\frac{u_\theta u_\phi}{\tan\theta}\right)}\right]. \tag{19}$$

3. Case of a thin Newtonian flow in a centrifugal zone

3.1. Thin centrifugal flow

To illustrate an application of the above averaged equations the particular case of a thin flow ($h/r\ll 1$) in a centrifugal zone ($Ro\ll 1$) is now considered. In this case it can be assumed that $\theta\approx\beta$ and that $u_\phi\gg u_r>u_\theta$. In addition it will be assumed that the influence of gravity can be neglected (i.e. $g\ll\Omega^2 r\sin\beta$). A relative angular velocity $\omega'=\Omega-\omega$ is defined where $\omega'/\Omega\ll 1$ such that

$$u_\phi=(\Omega-\omega')r\sin\beta\approx\Omega r\sin\beta. \tag{20}$$

Given these assumptions the momentum Eqs. (17)–(19) may be simplified as follows. For the left-hand side recall that $\lambda\approx(h/r)\sin\beta$ for a thin flow. On the right-hand side all terms except those involving u_ϕ may be neglected. Eqs. (17)–(19) therefore reduce to

$$\frac{\partial\bar{\tau}_{r\theta}}{\partial r}+\frac{\partial h}{\partial r}\frac{(\bar{\tau}_{r\theta}-\tau_{r\theta}|_h)}{h}+\frac{(\sigma_\theta|_0-\sigma_\theta|_h)}{h}\approx-\rho\Omega^2 r\sin\beta\cos\beta, \tag{21}$$

$$\frac{\partial\bar{\sigma}_r}{\partial r}+\frac{\partial h}{\partial r}\frac{(\bar{\sigma}_r-\sigma_r|_h)}{h}+\frac{(\tau_{r\theta}|_0-\tau_{r\theta}|_h)}{h}\approx-\rho\Omega^2 r\sin^2\beta, \tag{22}$$

$$\frac{\partial \overline{\tau}_{r\phi}}{\partial r}+\frac{\partial h}{\partial r}\frac{(\overline{\tau}_{r\phi}-\tau_{r\phi}|_h)}{h}+\frac{(\tau_{\theta\phi}|_0-\tau_{\theta\phi}|_h)}{h}\approx\rho\sin\beta\left[\left(2\overline{u}_r+\frac{\overline{u}_\theta}{\tan\beta}\right)\Omega-\overline{u_r\frac{\partial\overline{\varpi}'}{\partial r}r}\right]. \tag{23}$$

Note that mean and boundary stresses have been assumed to be of the same order of magnitude and rates of change of stress and flow thickness are not neglected.

3.2. Newtonian fluid

To make further progress a constitutive law is required. For Newtonian viscous flow the deviatoric stress tensor **S** is related to the velocity strain rate tensor **D** by

$$\mathbf{S}=2\mu\mathbf{D}, \tag{24}$$

and this relationship also holds for the averaged quantities. To determine the strain rates it is necessary to assume a velocity profile through the thickness of the flow. An appropriate basis for this profile is the results provided by Makarytchev et al. (1997) for thin film flow in the centrifugal zone. Following the example of Bohr et al. (1993) it will be assumed that this velocity profile is scaleable by the mean velocity and independent of the flow surface gradient dh/dr.

The profile for the radial velocity is therefore a parabolic distribution (as obtained for Nusselt flow down an inclined plane) expressed as a function of the mean radial velocity $\overline{u}_r$

$$u_r=3\overline{u}_r\frac{s}{h}\left(1-\frac{1}{2}\frac{s}{h}\right). \tag{25}$$

The profile for the relative angular velocity ω' is scaled by the mean relative angular velocity $\overline{\varpi}'$ and is expressed as

$$\omega'=\frac{5}{2}\overline{\omega'}\frac{s}{h}\left(1-\frac{1}{2}\frac{s^2}{h^2}+\frac{1}{8}\frac{s^3}{h^3}\right). \tag{26}$$

Note that Eqs. (25) and (26) are obtained directly for Newtonian viscosity from the thin film, centrifugal case of Eq. (7): $\partial\tau_{r\theta}/\partial s=\rho\Omega^2 r\sin^2\beta$, and Eq. (8): $\partial\tau_{\theta\varphi}/\partial s=-2u_r\Omega\sin\beta$. In the thin-film approximation the through-thickness velocity component u_θ is neglected relative to the radial u_r and circumferential u_ϕ components. Nevertheless, Makarytchev et al. (1997) do also give an analytical expression for u_θ. However, their expression for u_θ is inconsistent with the surface streamline boundary condition (13a). This discrepancy is noted in passing here, but will be considered in more detail later in this paper. If boundary zones at inlet and outlet where the flow surface gradient dh/dr may not be small are to be considered, then an expression for u_θ that is consistent with both the streamline boundary conditions (13a,b) is required. However, since the averaged equations only require the mean value $\overline{u}_\theta$ it is sufficient to assume that this can be obtained as follows:

$$\overline{u}_\theta(r)\approx\frac{1}{2}\overline{u}_r\frac{h}{r}\left(1-\frac{r}{h}\frac{\partial h}{\partial r}\right). \tag{27}$$

The mean direct strain rates for a thin flow of Newtonian fluid are therefore

$$\overline{D}_r=\frac{\partial\overline{u}_r}{\partial r}+\frac{1}{2}\frac{\overline{u}_r}{r}\left[1-\frac{r}{h}\frac{\partial h}{\partial r}\right],\quad \overline{D}_\phi=\frac{\overline{u}_r}{r},\quad \overline{D}_\theta=-\frac{1}{2}\frac{\overline{u}_r}{r}\left[1-3\frac{r}{h}\frac{\partial h}{\partial r}\right]. \tag{28}$$

While the mean shear strain rates are

$$\overline{D}_{r\theta}=-\frac{3}{4}\frac{\overline{u}_r}{h},\quad \overline{D}_{\theta\phi}=\frac{25}{32}\overline{\varpi}'\frac{r}{h}\sin\beta,\quad \overline{D}_{r\phi}=\frac{1}{2}\left[\frac{9}{16}\overline{\varpi}'\left(\frac{\partial h}{\partial r}\frac{r}{h}-1\right)-\frac{\partial\overline{\varpi}'}{\partial r}r\right]\sin\beta. \tag{29}$$

Substitution of Eqs. (28) and (29) into the constitutive law (24) provides the through-thickness averaged shear stresses $\overline{\tau}_{r\theta}\equiv\overline{S}_{r\theta}$ and $\overline{\tau}_{r\phi}\equiv\overline{S}_{r\phi}$ required for the momentum Eqs. (21) and (23) and also the mean direct deviatoric stresses $\overline{S}_r$, $\overline{S}_\theta$, $\overline{S}_\phi$. The latter give the mean direct stresses with the addition of the hydrostatic stress $\overline{\sigma}_h\equiv(\overline{\sigma}_r+\overline{\sigma}_\theta+\overline{\sigma}_\phi)$, e.g. $\overline{\sigma}_r\equiv\overline{\sigma}_h+\overline{S}_r$.

The momentum equations also require expressions for the boundary stresses. At the base of the flow the shear tractions are

$$\tau_{r\theta}|_0=2\mu D_{r\theta}|_0=-3\mu\frac{\overline{u}_r}{h},\quad\text{and}\quad \tau_{\theta\phi}|_0=2\mu D_{\phi\theta}|_0=\frac{5}{2}\mu\overline{\varpi}'\frac{r}{h}\sin\beta. \tag{30}$$

To be consistent with the assumed velocity profiles (25) and (26) it is assumed that at the free surface of the flow the normal and shear tractions vanish, thus

$$\sigma_\theta|_h=\tau_{r\theta}|_h=\tau_{\theta\varphi}|_h=0. \tag{31}$$

It also follows that at the free-surface of the flow:

$$\sigma_r|_h\approx 0\ \text{and}\ \tau_{r\phi}|_h\approx-\frac{25}{16}\mu r\sin\beta\frac{\partial\overline{\varpi}'}{\partial r}. \tag{32}$$

A linear variation of the through-thickness stress σ_θ is assumed and therefore the mean value is half the interface contact pressure

$$\overline{\sigma}_\theta=\frac{1}{2}\sigma_\theta|_0. \tag{33}$$

The system of Eqs. (11a) and (21)–(33) collectively define a problem of two variables, $\overline{u}_r$ and $\overline{\varpi}'$, as functions of r that can be solved for inlet and outlet boundary conditions. The numerical results presented in this paper are obtained by the direct use of this full set of equations. However, the two coupled differential equations for $\overline{u}_r$ and $\overline{\varpi}'$ could be obtained explicitly, if required, as follows. Making use of Eqs. (11a, 24, 28, 29, 31, 33) and the identity $\overline{\sigma}_\theta\equiv\overline{\sigma}_h+\overline{S}_\theta$ the through-thickness momentum Eq. (21) can be solved to obtain the mean hydrostatic stress $\overline{\sigma}_h$ as a function of $\overline{u}_r$ and its derivatives. This expression for $\overline{\sigma}_h$ can then be substituted into the radial momentum Eq. (22) by recalling that $\overline{\sigma}_r\equiv\overline{\sigma}_h+\overline{S}_r$. With use of Eqs. (11a, 24, 28, 30–32) this can provide a single differential equation in $\overline{u}_r$. An equivalent differential equation in $\overline{\varpi}'$ can be obtained by substitution of Eqs. (11a, 24, 27, 29, 30, 31) into the circumferential momentum Eq. (23). Note that in this special case of flow in a centrifugal zone ($Ro\ll 1$) where $\omega'/\Omega\ll 1$ the differential equation for $\overline{u}_r$ is independent of $\overline{\varpi}'$. However, the differential equation for $\overline{\varpi}'$ is coupled since it does contain $\overline{u}_r$ terms.

3.3. Slender flow mid-zone

Bizard et al. (2011) have shown that in a centrifugal flow there will typically be a large mid-zone where the flow is independent of either inlet or outlet boundary conditions. In this mid-zone the rate of change of flow-thickness dh/dr is of the same order as h/r and the momentum Eqs. (21)–(23) reduce to

$$\sigma_\theta|_0\approx-\rho\Omega^2 rh\sin\beta\cos\beta,\quad \tau_{r\theta}|_0\approx-\rho\Omega^2 rh\sin^2\beta,\quad\text{and}\quad \tau_{\theta\phi}|_0\approx 2\rho h\overline{u}_r\Omega\sin\beta. \tag{34}$$

These equilibrium statements lead directly to algebraic expressions for the flow velocity and thickness. It is convenient to first define reference radial and angular velocities and a reference flow thickness

$$\overline{u}_{r,ref}=\left(\frac{Q^2\Omega^2}{12\pi^2\nu r_{in}}\right)^{1/3},\quad \overline{\varpi}'_{ref}=\frac{1}{5\sin^2\beta}\left(\frac{12Q^4\Omega}{\pi\nu^2 r_{in}{}^8}\right)^{1/3},\quad h_{ref}=\frac{1}{\sin\beta}\left(\frac{3Q\nu}{2\pi\Omega^2 r_{in}{}^2}\right)^{1/3}. \tag{35}$$

The mean radial and relative angular velocities and flow thickness in a centrifugal mid-zone can then be written

non-dimensionally as

$$\overline{U}=\frac{\overline{u}_r}{\overline{u}_{r,ref}}=R^{-(1/3)},\quad \overline{W'}=\frac{\overline{\omega}'}{\overline{\omega}'_{ref}}=R^{-(8/3)}\quad\text{and}\quad \frac{h}{h_{ref}}=R^{-(2/3)}\quad\text{where } R=\frac{r}{r_{in}}. \tag{36}$$

It is useful at this stage to comment on dimensionless groups and the relationships between them. The ratios h/r, $g/\Omega^2 r\sin\beta$ and the Rossby number Ro are useful dimensionless groups irrespective of the choice of constitutive law. It has been assumed that these three numbers are much less than unity, and for Newtonian viscous flow the Ekman number, Reynolds number and ratio of the relative angular velocity to that of the cone follow as:

$$Ek=\left(\frac{h_E}{h}\right)^2=\frac{1}{3Ro},\quad \mathrm{Re}=\frac{\overline{u}_r h}{\nu}=3Ro^2\frac{r}{h},\quad\text{and}\quad \frac{\overline{\omega'}}{\Omega}=\frac{12}{5}Ro^2, \tag{37a}$$

where

$$Ro=\frac{1}{\sin\beta}\left(\frac{Q^2}{12\pi^2\Omega\nu r^4}\right)^{1/3}\quad\text{and}\quad \frac{h}{r}=\frac{1}{\sin\beta}\left(\frac{3Q\nu}{2\pi\Omega^2 r^5}\right)^{1/3}. \tag{37b}$$

The choice of flow in a centrifugal zone therefore gives, as expected, a film thickness less than the Ekman thickness and an extremely small relative angular velocity.

3.4. Boundary conditions

3.4.1. Inlet boundary condition

A representative inlet flow in an industrial spinning cone machine is flow from a preceding conical surface of different apex angle, see Fig. 2. The preceding angle β_0 may be either greater or less than the main cone angle β. Examples of the two different possibilities are a spinning cone distillation column ($\beta_0>\beta$) and a conical centrifugal filter ($\beta_0<\beta$). If the inlet cone is also operating in a thin-film centrifugal regime then Eqs. (35) and (36) can provide the inlet boundary conditions for the second cone. Note that $r_0\sin\beta_0=r_{in}\sin\beta$ and make the assumption that the flow thickness is continuous at the transition point. The inlet velocity boundary conditions for the second cone can then be

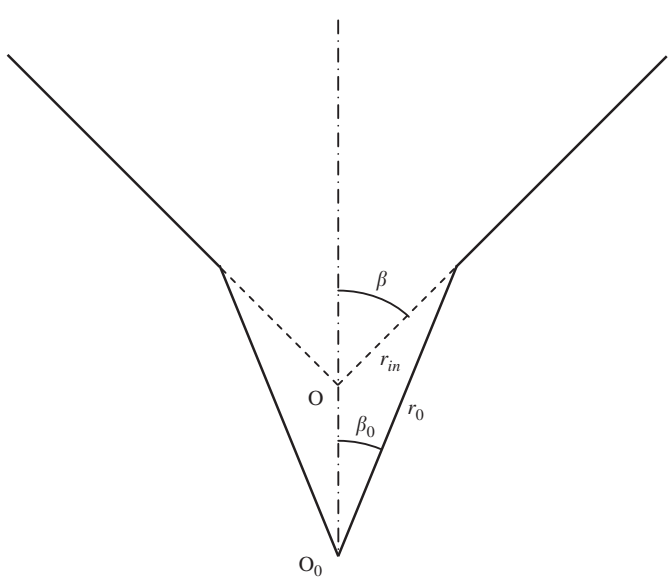

Fig. 2. Geometry of inlet and main cone.

defined in its own co-ordinate system as

$$\overline{U}_{inlet}=\frac{\overline{u}_{r,inlet}}{\overline{u}_{r,ref}}=\left(\frac{\sin\beta_0}{\sin\beta}\right)^{1/3}\quad\text{and}\quad \overline{W}'_{inlet}=\frac{\overline{\omega}'_{inlet}}{\overline{\omega}'_{ref}}=\left(\frac{\sin\beta_0}{\sin\beta}\right)^{2/3}. \tag{38}$$

A transition from an inlet cone $\beta_0=12.5^\circ$ to a main cone $\beta=25^\circ$ for example would therefore be expected to give inlet flow velocities to the main cone of $\overline{U}_{inlet}=0.8$ and $\overline{W}'_{inlet}=0.64$. Irrespective of the inlet boundary conditions the flow is expected to rapidly converge to the mid-zone conditions. The rate of this convergence can be determined by solution of the averaged equations outlined in this paper.

3.4.2. Outlet boundary condition

A typical conical centrifuge has a free outlet at the top of the cone. Beyond this point the interface contact pressure and shear tractions vanish so that $\sigma_\theta|_0=\tau_{r\theta}|_0=\tau_{\theta\phi}|_0=0$. The rate of flow thinning dh/dr immediately downstream of the exit of the cone r_{out} also becomes very large and consequently the momentum Eqs. (24) and (25) reduce to the outlet boundary conditions

$$\frac{\partial h}{\partial r}\frac{\overline{\sigma}_r}{h}\approx-\rho\Omega^2 r\sin^2\beta\quad\text{and}\quad \frac{\partial h}{\partial r}\frac{\overline{\tau}_{\varphi r}}{h}\approx 2\rho\overline{u}_r\Omega\sin\beta\quad\text{at } r=r_{out}. \tag{39}$$

4. Comparison of averaged equations with 2D CFD

In order to investigate the accuracy of the averaged equations outlined above numerical results are now compared to those obtained using a commercial CFD software package. The comparison also allows the assumptions regarding the through-thickness velocity profiles and the outlet boundary conditions to be tested.

4.1. Numerical method for averaged equations

Numerical solutions to the averaged equations for the case of a slender Newtonian flow in a centrifugal zone have been obtained using a Matlab (MATHWORKS, 2008) script. The script provides a solution for $\overline{u}_r(r)$ and $\overline{\omega}'(r)$ for the system of Eqs. (11a) and (21)–(33) to match prescribed inlet and outlet boundary conditions.

The centrifuge domain is discretized between inlet r_{in} and outlet r_{out}. An initial estimate of $\overline{u}_r(r)$ and $\overline{\omega}'(r)$ must be provided, an appropriate estimate being the mid-zone solutions (36). Continuity (11a) is imposed throughout to obtain $h(r)$ and therefore the strain rates (28) and (29) and the deviatoric stresses **S** can be found. Substitution of the deviatoric stresses and boundary stress values (30)–(33) allows the momentum Eqs. (21)–(23) to be solved to obtain residuals (errors) based on the current estimates of $\overline{u}_r(r)$ and $\overline{\omega}'(r)$. These residuals are treated as accelerations and an explicit Euler time stepping method is adopted to iteratively progress to a converged solution. Convergence is checked by monitoring the RMS value of the residuals for the whole domain.

Four boundary conditions are required in total: two inlet velocities $\overline{u}_r(r_{in})$ and $\overline{\omega}'(r_{in})$and two outlet stresses $\overline{\sigma}_r(r_{out})$and $\overline{\tau}_{\phi r}(r_{out})$. For stability these boundary conditions are applied gradually (over a large number of time steps) by linear adjustment from starting values, determined by the initial estimate of $\overline{u}_r(r)$ and $\overline{\omega}'(r)$, to the final required boundary values.

4.2. CFD method

4.2.1. Software and solution method

Two-dimensional CFD simulations have been carried out using the STAR-CD package (CD-adapco, 2009). The STAR-CD "multi-fluid"

option is used to model the free-surface flow problem. This is a volume-of-fluid (VOF) method which is appropriate for immiscible fluids where the fluids are separated by a smooth interface possessing a characteristic length scale comparable with that of the solution domain. Two fluids are modeled: the primary dense, viscous liquid and a gas (air). The density and viscosity of the air are approximately three and five orders of magnitude less, respectively, than those of the liquid. Both fluids are modeled as incompressible and surface tension is neglected. A transient simulation is used with a constant input flow rate of fluid to obtain a converged steady state result. A rotating reference frame is used for the simulation (although identical results were obtained in test simulations with a static reference frame and moving walls). Solution method parameters are summarized in Table 1.

4.2.2. Mesh

STAR-CD does not provide for two-dimensional meshes so an axi-symmetric solution is obtained by use of a mesh a single element wide with cyclic boundary conditions for rotational symmetry about the vertical axis. It is unnecessary to model the entire inner volume of the centrifuge and therefore the mesh only covers the area of interest which is a thin layer above the centrifuge cone wall. The standard mesh used consisted of approximately 7500 cuboid elements ($150\times50\times1$ in the r,θ,ϕ directions, respectively).

An example mesh is shown in Fig. 3. In order to speed up convergence of the transient simulation to a steady state solution an initial, approximate, fluid distribution is defined. The outer surface of the mesh ($\theta=\beta$) represents the centrifuge wall and is an impervious, no-slip surface. The inner surface of the mesh is a static pressure boundary condition ($p=0$) that allows flow of the

Table 1
STAR-CD (CD-adapco) CFD solution method settings.

Solution method	Multi-fluid, Transient, SIMPLE algorithm, Double precision
Max. residual tolerance	0.001, Max number of outer iterations:10
Solver type:	Scalar, Scalar method: AMG
Temporal discretization:	Euler implicit, constant time step=0.001 s
Flow variables:	*u v w* momentum only, no turbulence
Primary variables: *u v w*:	Relax. factor 0.7, number of sweeps 100, residual tol. 0.1
Primary variables: Pressure:	Relax. factor 0.3, number of sweeps 1000, resid. tol. 0.05
Primary variable differencing	Central, blending method fixed with a factor of 1
Scalars:	Under-relaxation fac. 0.8, max. sweeps 100, resid. tol. 0.1
Scalars: Differencing	Scheme HRIC, blending method fixed with a factor of 0.95
Scalars: Solution method:	Transport, Buoyancy on, Constant density

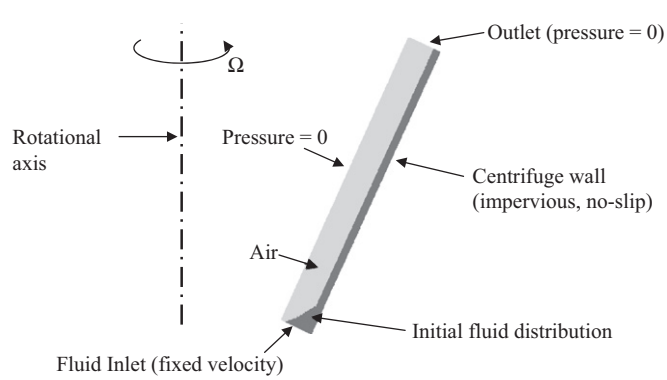

Fig. 3. CFD model of flow in conical centrifuge flow.

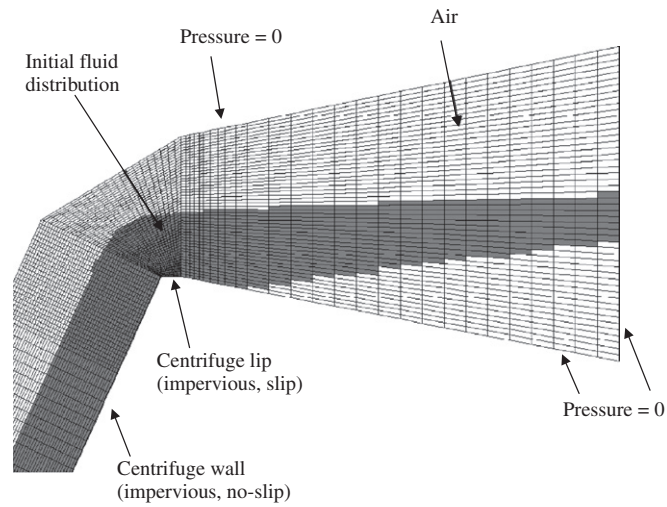

Fig. 4. Detail of CFD mesh at outlet for free-overfall.

secondary fluid (air). At the inlet surface a velocity distribution is prescribed consistent with the required constant inlet volumetric flow rate Q and mean velocities $\overline{u}_r(r_{in})$ and $\overline{\omega}'(r_{in})$. At both inlet and outlet the mesh is refined in the radial direction in order to better capture the boundary effects.

Two alternative mesh configurations were used at outlet. The first, shown in Fig. 3, is a simple pressure condition of $p=0$ on a surface locally perpendicular to the cone wall. The second, shown in detail in Fig. 4, explicitly models the free-overfall at the centrifuge lip. A small, finite, lip is modeled as an impervious surface but allowing slip. The remaining surfaces of the extended mesh are pressure boundary conditions of $p=0$.

4.2.3. Simulation parameters

Three simulation configurations were investigated, each with the same reference Reynolds number Re=0.159, but with different ratios of h/r. The parameter sets adopted for the three configurations (A, B and C) are detailed in Table 2. Note that for all the configurations the Rossby number is $Ro<0.1$ and $g/\Omega^2 r_{in}\sin\beta<0.01$. All three sets therefore represent flows in a centrifugal zone where the effect of gravity is negligible relative to the centripetal acceleration. Set A is the most slender flow with $h_{ref}/r_{in}=0.0074$. Set B and set C are flows where h_{ref}/r_{in} is 5 and 10 times greater, respectively.

For each configuration arbitrary inlet boundary conditions have been selected of $\overline{W}'_{in}=0$ and $\overline{U}_{in}\sim0.85$, while the outlet boundary condition is intended to represent a free overfall. For configuration set A two alternative implementations of these boundary conditions are used at both inlet and outlet. At inlet the prescribed velocity u_r has either a parabolic profile (25), or a uniform profile, i.e. $u_r=\overline{u}_r$. The outlet boundary condition is either the simple pressure boundary condition $p=0$ at $r=r_{out}$, or the free overfall is explicitly modeled (Fig. 4).

4.2.4. Check of solution accuracy

As the CFD solution method adopted was transient it was necessary to run simulations for a sufficient length of simulated real time in order to obtain converged steady state results. Simulation runs of 3 s were judged to be adequately converged. In a typical simulation the flow thickness at a point in the mid-zone of the cone was within 1% of its final (3 s) value after 0.3 s and within 0.01% after 0.8 s.

To investigate the sensitivity of the solution to mesh density additional test simulations were carried out with the mesh

Table 2
STAR-CD simulation parameter sets.

Simulation parameter set	Set A	Set B	Set C
Flow rate Q (m^3/s)	500×10^{-6}	73.5×10^{-6}	147×10^{-6}
$\nu=\mu/\rho$ (m^2/s)	0.005	0.00368	0.00735
Cone angle β (deg.)	25	25	25
$r_{in}\sin\beta$ (m)	0.1	0.02	0.02
Spin rate Ω (rpm)	2181	3586	2535
Reference flow velocity at inlet $\overline{u}_{r,ref}$ (m/s)	0.453	0.333	0.333
Reference flow thickness at inlet h_{ref} (mm)	1.76	1.76	3.51
h_{ref}/r_{in}	0.0074	0.037	0.074
Rossby number $Ro=\overline{u}_r/\Omega r\sin\beta$	0.020	0.044	0.063
$\overline{U}_{in}=\overline{u}_{r,in}/\overline{u}_{r,ref}$	0.8	0.84	0.89
$g/\Omega^2 r_{in}\sin\beta$	0.0019	0.0035	0.0070
$\overline{W}'_{in}=\overline{\omega}'_{inlet}/\overline{\omega}'_{ref}$	0	0	0
Reynolds number $\mathrm{Re}=\overline{u}_r h/\nu=3Ro^2 r/h$	0.159	0.159	0.159
r_{out}/r_{in}	1.2	2	2
Inlet velocity distribution	Parabolic or uniform	Parabolic	Parabolic
Outlet boundary condition	Free overfall or $p=0$	$p=0$	$p=0$

Fig. 5. Liquid volume fraction (set A).

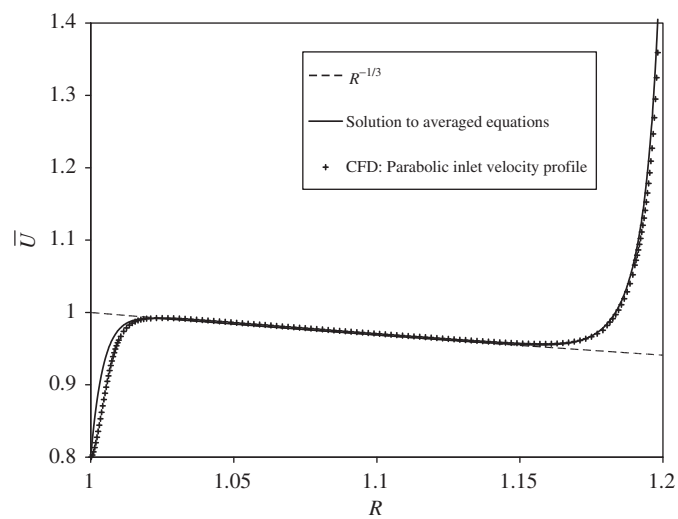

Fig. 6. Radial variation of mean radial velocity (set A, $h_{ref}/r_{in}=0.0074$).

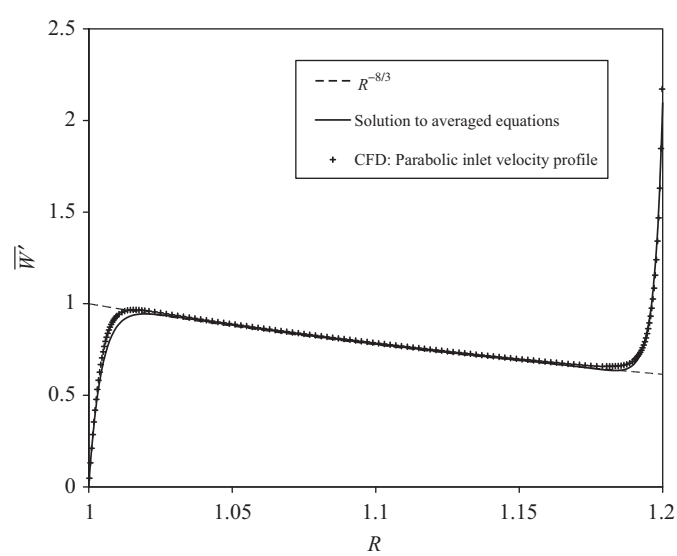

Fig. 7. Radial variation of mean relative angular velocity (set A, $h_{ref}/r_{in}=0.0074$).

density doubled in both the through-thickness and radial directions. The results for the increased mesh density showed a negligible difference to the original mesh: e.g. less than 0.05% difference in the mean velocity of the flow.

4.3. Results

4.3.1. Radial variation of mean velocities

Fig. 5 shows a typical converged flow result for a free-overfall CFD simulation using the parameter set A. The figure shows contours of volume fraction of liquid. Within the main part of the centrifuge the CFD VOF method achieves a fairly precise realization of the liquid free-surface with a steep variation of liquid volume fraction from 1 to 0 over only a few elements. However, after the outlet r_{out} the reduction in real flow thickness is very rapid and the free-surface is less distinct.

Figs. 6 and 7 compare the solution to the averaged equations to the two-dimensional CFD simulation for parameter set A. The

figures show the mean radial velocity $\overline{U}$ and mean relative angular velocity $\overline{W'}$, respectively. Both averaged equations and CFD solutions converge to $\overline{U}=R^{-1/3}$ and $\overline{W'}=R^{-8/3}$ in the flow mid-zone. Close to r_{in} and r_{out} the flow is influenced by the inlet and outlet boundary conditions. The inlet boundary conditions for both models are the arbitrary selection of $\overline{U}_{in}=0.8$ and $\overline{W'}_{in}=0$. However, for the outlet a different approach is taken for each model: the boundary conditions of Eq. (39) are applied to the averaged equations whereas for the CFD the free-overfall is explicitly modeled (Fig. 4). Figs. 6 and 7 show the very good agreement of the two models and boundary conditions at the outlet.

Fig. 8 shows the variation of $\overline{U}$ in the inlet zone in more detail and also compares the averaged equation solution to two CFD models with alternative inlet velocity profiles: parabolic and uniform. Although the averaged equation approach does not provide an exact match to either CFD model the prediction of the length of the inlet influenced zone is excellent and the error is of the same order as the difference between the two CFD models.

Fig. 9 compares the results for $\overline{U}$ obtained with the alternative approaches to modeling the centrifuge outlet. The pressure boundary condition of $p=0$ at $r=r_{out}$ gives a slightly lower outlet velocity than the explicitly modeled free-overfall but still provides a reasonable approximation to the flow acceleration at outlet. The $p=0$ boundary condition is adopted with parameter sets B and C.

4.3.2. Comparison for less slender flows

The CFD simulations with parameter sets B and C are intended to test the accuracy of the averaged equation approach for thicker flows. Figs. 10 and 11 compare solutions to the averaged equations with CFD results for B and C, respectively. The accuracy of the approximate averaged equation approach is tested in the inlet zone. Although set A ($h_{ref}/r_{in}=0.0074$) shows a good agreement of the averaged equations to the CFD results in the inlet zone the match is less accurate for set B ($h_{ref}/r_{in}=0.037$), and worse for set C ($h_{ref}/r_{in}=0.074$). This breakdown of accuracy for thicker flows is expected since the averaged equation approach has been based on the presumption of a slender flow, i.e. $h/r \ll 1$. However, it is surprising that even for such a relatively thick flow as set C the

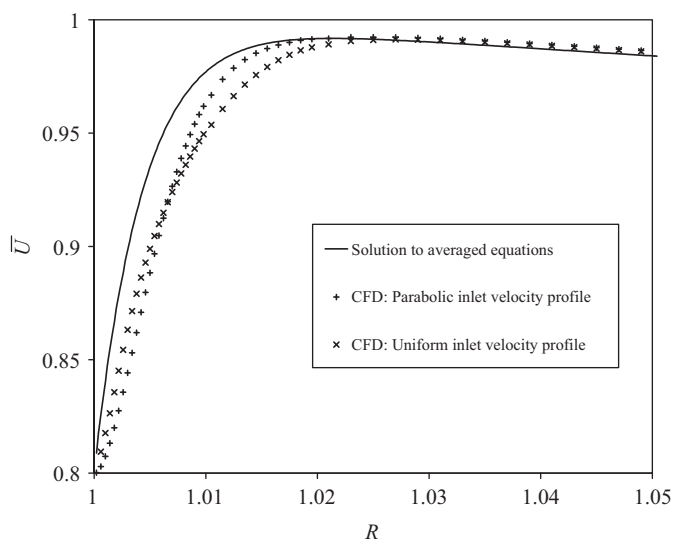

Fig. 8. Sensitivity to inlet radial velocity profile (set A).

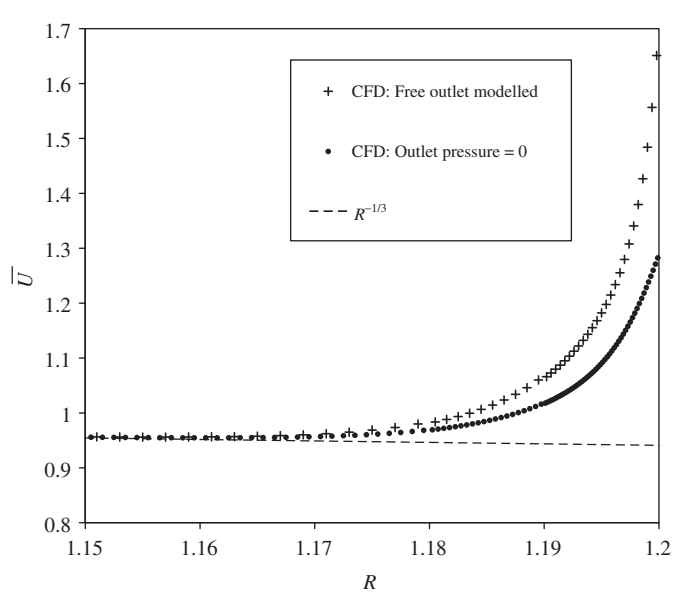

Fig. 9. Sensitivity to outlet boundary condition (set A).

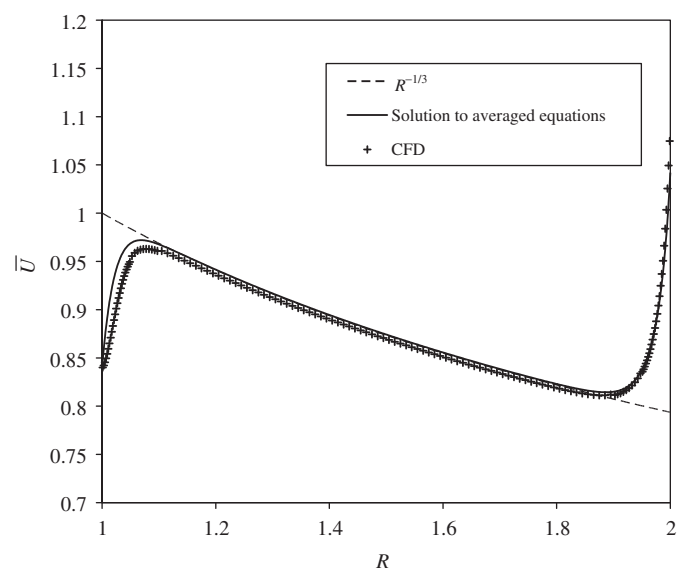

Fig. 10. Radial variation of mean radial velocity (set B, $h_{ref}/r_{in}=0.037$).

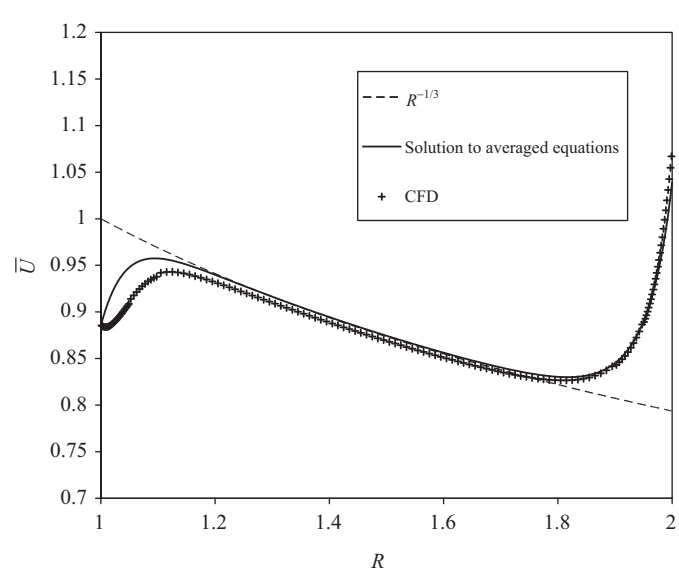

Fig. 11. Radial variation of mean radial velocity (set C, $h_{ref}/r_{in}=0.074$).

averaged equations still provide a very good match for the behavior at outlet.

4.3.3. Through-thickness velocity distribution

It is instructive to compare through-thickness velocity profiles obtained by CFD with the thin-film theory of Makarytchev et al. (1997). Although the components of the velocity are of different magnitudes it is convenient to present the profiles on a single plot. Each velocity component will therefore be normalized by its magnitude at the free surface.

The thin-film theoretical profiles for the radial and circumferential components of the velocity (u_r and the relative angular velocity ω') are given in the expressions (25), (26), (35) and (36) above. These velocity and angular velocity profiles are non-dimensionalised as follows:

$$U_r = \frac{2}{3}\frac{u_r}{\overline{u}_r} \quad \text{giving} \quad U_{r,theory} = 2\frac{s}{h}\left(1-\frac{1}{2}\frac{s}{h}\right), \tag{40}$$

$$U'_\phi = \frac{16}{25}\frac{\varpi'}{\overline{\varpi'}} \quad \text{giving} \quad U'_{\phi,theory} = \frac{8}{5}\frac{s}{h}\left(1-\frac{1}{2}\frac{s^2}{h^2}+\frac{1}{8}\frac{s^3}{h^3}\right), \tag{41}$$

where $U_{r,theory}$ and $U'_{\phi,theory}$ are the theoretical profiles for thin-film flow in a centrifugal zone given by Makarytchev et al. (1997). At the surface of the flow $s=h$ and therefore $U_{r,theory} = U'_{\phi,theory} = 1$.

Now consider the magnitude of the through-thickness velocity component at the free-surface $u_\theta|_h$. Examination of Eqs. (35) and (36) reveals that for mid-zone slender flow the gradient of the free-surface is

$$\frac{\partial h}{\partial r} = -\frac{2}{3}\frac{h}{r}, \tag{42}$$

and it therefore follows from Eq. (13a) that the surface streamline direction is such that

$$u_\theta|_h = \left(\frac{h}{r}-\frac{\partial h}{\partial r}\right)u_r|_h = \frac{5}{3}\frac{h}{r}u_r|_h = \frac{5}{2}\frac{h}{r}\overline{u}_r. \tag{43}$$

The non-dimensional form of u_θ consistent with Eqs. (40) and (41) is therefore

$$U_\theta = \frac{2}{5}\frac{r}{h}\frac{u_\theta}{\overline{u}_r}. \tag{44}$$

This should provide $U_\theta=1$ at the surface of the flow.

However, in their thin film approximation Makarytchev et al. (1997) calculate that

$$u_{\theta,theory} = \frac{\Omega^2\sin^2\beta}{\nu}s^2\left(\frac{7}{6}h-\frac{1}{2}s\right), \tag{45}$$

and therefore

$$U_{\theta,theory} = \frac{6}{5}\left(\frac{s}{h}\right)^2\left(\frac{7}{6}-\frac{1}{2}\frac{s}{h}\right). \tag{46}$$

It is clear that at the surface ($s=h$) of the flow their $U_{\theta,theory}=4/5$, and not unity as expected (i.e. an error of 20%). Although the error in $u_{\theta,theory}$ is only of the order of $u_r h/r$, because u_θ is itself of the same order this is a significant inaccuracy. The error arises because of the boundary layer approximation adopted by Makarytchev et al. (1997) from the outset, i.e. that $h/r \ll 1$.

Fig. 12 compares CFD results for parameter set A (the most slender set) to the thin-film theory. The CFD velocity profiles are obtained from the mid-zone of the flow at $R=1.1$. The CFD result for U_r is an excellent match to the theoretical parabolic profile. The relative circumferential velocity U'_ϕ is also in very good agreement with the theory. The CFD results for the through-thickness velocity U_θ match expectations with $U_\theta \approx 1$ at the flow surface but do not, as explained above, match the thin film theory ($U_{\theta,theory}=0.8$ at the flow surface).

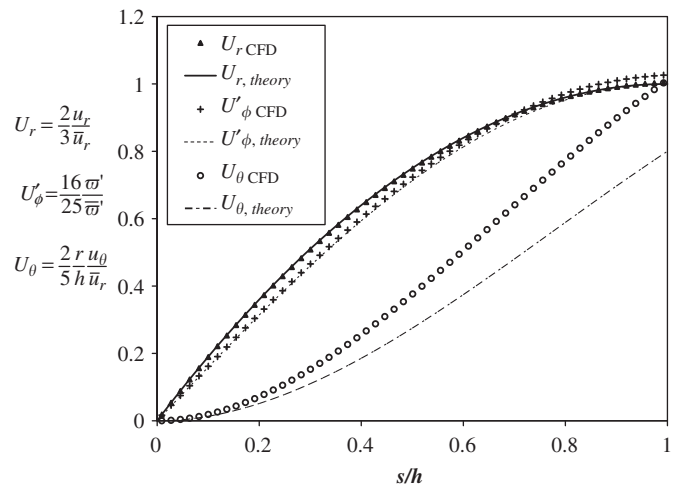

Fig. 12. Through-thickness velocity profiles, CFD compared to thin-film theory (set A).

5. Conclusion

In this paper a set of through-thickness averaged equations for momentum and strain rate are derived for the problem of axisymmetric free-surface flow within a spinning cone. These expressions are independent of the choice of constitutive law and can be used for modeling the flow distribution of a variety of materials within industrial conical centrifuges. The approach has been validated for the particular case of a thin Newtonian viscous flow by comparison with converged results obtained from a commercial CFD package. The averaged equations give an accurate prediction of flow thickness and velocity and of the radial influence of inlet and outlet boundary conditions. Comparison of the CFD results for the through-thickness variation of flow velocity with a theoretical boundary layer approximation shows good agreement for radial and circumferential components. However, it is shown that if the boundary layer approximation is also used to derive an expression for the very small through-thickness velocity component then an error of 20% arises.

Nomenclature

A	cross-sectional area of the flow
$\mathbf{D}$	velocity strain rate tensor
D_{ij}	strain rate component
Ek	Ekman number
f	a general function
$\overline{f}$	through-thickness (area) average of any function f
g	acceleration due to gravity
h	flow thickness
h_E	Ekman layer thickness
p	pressure
Q	volumetric flow rate
R	non-dimensional radial co-ordinate
Re	Reynolds number
Ro	Rossby number
$\mathbf{S}$	deviatoric stress tensor
S_{ij}	deviatoric stress component
s	through-thickness co-ordinate
t	time
u_i	velocity component
U	non-dimensional radial velocity
W'	non-dimensional relative angular velocity

r,θ,ϕ	spherical co-ordinate system with origin at (theoretical) apex of cone
β	cone semi-angle
λ	flow slenderness function
μ	dynamic viscosity
ν	kinematic viscosity
ρ	density
σ_i	direct stress component
τ_{ij}	shear stress component
Ω	angular velocity of cone
ϖ	angular velocity of flow
ϖ'	angular velocity of flow relative to cone

Subscripts

0	referring to preceding (inlet) cone
ref	reference value
in	inlet
out	outlet
theory	referring to a thin-film theoretical value

Acknowledgments

Much of this work was carried out during a sabbatical visit to the Fluid Mechanics group of the Mechanical Engineering Department at the Danish Technical University. I would like to thank all of DTU for their hospitality, but in particular Jens Nørkær Sørensen, Jens Honore Walther and Thomas Bohr for their patient help and input. I would also like to acknowledge the contributions of colleagues in the Cambridge University Engineering Department: Arnaud Bizard, Norman Fleck and Peter Davidson, as well as the very helpful industrial perspective of Clive Grimwood of Thomas Broadbent & Sons.

References

Bizard, A.F., Symons, D.D., Fleck, N.A., Durban, D., 2011. Flow of damp powder in a rotating impervious cone. Journal of Applied Mechanics *78*, *021017*.
Bohr, T., Dimon, P., Putkaradze, V., 1993. Shallow-water approach to the circular hydraulic jump. Journal of Fluid Mechanics 254, 635–648.
Bruin, S., 1969. Velocity distributions in a liquid film flowing over a rotating conical surface. Chemical Engineering Science 24, 1647–1654.
Fung, Y.C., Tong, P., 2001. Classical and Computational Solid Mechanics. World Scientific Publishing Co, Singapore.
Makarytchev, S.V., Xue, E., Langrish, T.A.G., Prince, R.G.H., 1997. On modeling fluid flow over a rotating conical surface. Chemical Engineering Science 52 (6), 1055–1057.
Makarytchev, S.V., Langrish, T.A.G., Prince, R.G.H., 1998. Structure and regimes of liquid film flow in spinning cone columns. Chemical Engineering Science 53 (8), 1541–1550.
Matlab MATHWORKS, 2008. Matlab 7.6.0.324 (r2008a). The MathWorks Inc., 3 Apple Hill Drive, Natick, MA 01760-2098, USA.
STAR-CD package, CD-adapco, 2009. STAR-CD 4.08. CD-adapco, 60 Broadhollow Road, Melville, NY 11747, USA.
Watanabe, S., Putkaradze, V., Bohr, T., 2003. Integral methods for shallow free-surface flows with separation. Journal of Fluid Mechanics 480, 233–265.
White, F.M., 1991. Viscous Fluid Flow 2nd edition McGraw-Hill, USA.